Research Article

Time-space variability of satellite chlorophyll-*a* in the Easter Island Province, southeastern Pacific Ocean

Isabel Andrade[1], Samuel Hormazábal[1] & Marco Correa-Ramírez[1]
[1]Escuela de Ciencias del Mar
Pontificia Universidad Católica de Valparaíso, P.O. Box 1020, Valparaíso, Chile

ABSTRACT. The Easter Island Province (EIP) encompasses Easter Island (EI) and Salas y Gómez Island (SGI), which are located in the eastern boundary of the south Pacific subtropical gyre. This province is one of the most oligotrophic region in the world ocean with a high degree of endemism and distinguished by having the clearest waters in the world. Issues related to the biophysical coupling that sustains biological production in this region are still poorly understood. Satellite data compiled over a ten year period was used to characterize the spatial and temporal chlorophyll-*a* (Chl-*a*) variability around the EIP and determine the relationship between Chl-*a* and several physical forcing. Results shows a clear Chl-*a* annual cycle around the EIP, with maximum concentration during the austral winter. Chl-*a* spatial distribution shows a strong zonal dipole over EI that divides the island into two zones: southeast and northwest. Due to its small size and low elevation of SGI, it does not generate a significant local effect in Chl-*a* concentration, but a Chl-*a* increase is observed southeast of this island (~2 km) associated to a seamount. The mean geostrophic current in the EIP flows eastward, associated with the southeastern boundary of the subtropical gyre. However, recurrent mesoscale eddies traveling northwestward and produce large surface current variability with periods of high velocities in opposite direction. In the spring, wakes of high Chl-*a* concentration can be observed over EI, associated with the generation and detachment of submesoscale eddies from EI, which could have important biological implications during periods of low regional biological production.

Keywords: satellite chlorophyll-*a*, mesoscale and submesoscale eddies, subtropical anticyclonic gyre, Easter Island, Salas y Gómez Island, southeastern Pacific.

Variabilidad espacio-temporal de la clorofila-*a* satelital en la Provincia de Isla de Pascua, Océano Pacífico suroriental

RESUMEN. La Provincia de Isla de Pascua (PIP) está compuesta por las islas de Pascua (IP) y Salas y Gómez (ISG). Ambas islas se sitúan en el límite oriental del giro subtropical del Pacífico sur. Esta provincia es una de las regiones más oligotróficas en el océano mundial con un alto grado de endemismo y se distingue por tener las aguas más transparentes del mundo. Los aspectos relacionados con el acoplamiento biofísico que dan sustento a la producción biológica de esta región, son escasamente conocidos. Se utilizaron 10 años de información satelital para caracterizar la variabilidad espacial y temporal de la clorofila-*a* (Clo-*a*) alrededor de la PIP, y determinar su relación con los distintos forzantes físicos. Los resultados muestran un marcado ciclo anual de la Clo-*a* alrededor de la PIP, con mayores concentraciones durante invierno. La distribución espacial de la Clo-*a*, muestra un marcado dipolo zonal en IP que divide a la isla en una zona sureste y otra noroeste. La ISG, debido a su pequeño tamaño y escasa altura, no genera un efecto local significativo sobre las concentraciones de Clo-*a*. Sin embargo, al sureste de esta isla (~2 km), se presenta un notable incremento de Clo-*a* asociado a la presencia de un monte submarino. La corriente geostrófica promedio alrededor de la PIP presenta un flujo promedio hacia el este, característico del límite sureste del giro subtropical. Sin embargo, se observa una presencia frecuente de remolinos de mesoescala que viajan en dirección noroeste produciendo una alta variabilidad con períodos de intensas corrientes en dirección contraria. En IP, durante primavera, se observan estelas con alta concentración de Clo-*a* vinculadas a la formación y desprendimiento de remolinos de submesoescala desde la isla, lo que tendría importantes implicancias biológicas, especialmente durante los periodos de baja concentración de Clo-*a* a escala regional.

_____

Corresponding author: Isabel Andrade (isabelandradec@gmail.com)

INTRODUCTION

The Easter Island Province (EIP) is located on the eastern boundary of the south Pacific anticyclonic subtropical gyre, which governs the main features of oceanic surface circulation in the area. The geostrophic currents observed around the EIP flow predominantly northeast (Moraga *et al.,* 2010). Due the great distance that separates the EIP from the continent, the biodiversity around its shores presents the highest degree of endemism (*e.g.,* ~40% fish) of all oceanic islands off Chile coast (Parin *et al.,* 1991). The biological importance of this region is supported by the observed increase in coastal phytoplankton biomass respect to the oligotrophic subtropical gyre, which has been described as the clearest waters in the world (Pizarro *et al.,* 2006).

The subtropical gyre is an oligotrophic region with very low chlorophyll-*a* (Chl-*a*) concentrations in which the phytoplankton community is dominated by species of picoplankton (*e.g.,* prochlorophytes and cyanophytes) and nanoplankton (Ras *et al.,* 2008). This region is characterized by a deep pycnocline and strong horizontal gradients, which create a limited supply of nutrients to the euphotic zone, low primary productivity rates and high pCO_2 levels throughout the year (Hardy *et al.,* 1996). However, the link between physical and biological variability within the gyre occurs at several spatial and temporal scales that are not yet fully understood. The location of the dynamic center of the subtropical gyre, the region with a highest dynamic altitude of the sea level observed by satellite altimeters and where the pycnocline is deepest, does not geographically coincide with the location of the satellite Chl-*a* minimum (McClain *et al.,* 2004). Besides, high phytoplankton growth rates have been observed, which do not produce significant changes in phytoplanktonic carbon biomass in the subtropical gyres (Laws *et al.,* 1987; Marra & Heinemann, 1987; Marañon *et al.,* 2000, 2003). Indeed, the low phytoplanktonic biomass variability throughout the annual cycle and the seasonal increases in satellite Chl-*a* have mainly been attributed to the community's photo-adaptation in this region, since the largest Chl-*a* values occur during winter when the mixed layer is deep, ZNO_3 is relatively shallow, and there are lower light levels imposed by deeper mixing (McClain *et al.,* 2004). It has been stated that much of the phytoplanktonic biomass variability, the biological production and the export in the Pacific subtropical gyres, responds to low frequency climate variability such as El Niño and the decadal oscillation in the Pacific Ocean (Karl *et al.,* 2001). But the high frequency increases observed in Chl-*a* around oceanic islands could have a deep biological impact that has not been previously addressed.

Chl-*a* measurements performed around EIP during the 1999-2000 spring period by the Oceanic Islands cruise Cimar-5 show low surface Chl-*a* concentrations (<0.1 mg m^{-3}) surrounding Easter Island (EI), with the maximum (0.1 mg m^{-3} at 50 m) located just below the surface. Moreover, it has been observed that the water adjacent to Salas y Gómez Island (SGI) shows homogeneous Chl-*a* values (<0.05 mg m^{-3}) in the first 100 m of depth (Pizarro *et al.,* 2006). Satellite Chl-*a* data (SeaWifs datasets) for the same period show maximum values of between 0.03-0.05 mg m^{-3} in surface waters surrounding EI (Pizarro *et al.,* 2006), which is two orders of magnitude lower than Chl-*a* concentrations (~10 mg m^{-3} average) found in the southeastern Pacific upwelling and several times higher than Chl-*a* concentrations found in the ocean waters of the subtropical gyre (<0.001 mg m^{-3}). Although *in situ* Chl-*a* concentration measurements for the region are sparse, they suggest that the presence of islands and seamounts in the EIP could promote local processes of surface water enrichment and may have important implications on the transference of energy to higher trophic levels and the balance of nutrients and biological productivity within the region.

Local increases in phytoplankton biomass observed in the coastal waters of oceanic islands is called "Island Mass Effect" (IME; Doty & Ogury, 1956). These increases in phytoplankton are promoted by the interaction between physical forcing (*e.g.,* wind and currents) and the topography of the island, promoting the injection of macro and micronutrients into the euphotic zone and stimulating biological production. The formation of meso and submesoscale eddies is one of the mechanisms resulting from this interaction (Heywood *et al.,* 1990, 1996; Sangrà *et al.,* 2007; Hasegawa *et al.,* 2009), which, through their formation

and subsequent detachment from the islands, promote the vertical movement of nutrients, generating high surface or subsurface Chl-*a* concentrations within their surrounding waters (Sangrà *et al.,* 2007; Hasegawa *et al.,* 2009; Andrade *et al.,* 2014). These processes may have important effects on the success of larval recruitment in some species of pelagic fish and fish productivity in general around the island (Signorini *et al.,* 1999; Landaeta & Castro, 2004).

Regional balances have shown that mesoscale eddies may be responsible for a significant fraction (>20%) of ocean productivity, particularly in oligotrophic waters (Falkowski *et al.,* 1991). In the southeastern Pacific Ocean it has been argued that ~50% of the oceanic satellite Chl-*a* may be associated with the propagation of mesoscale eddies from the continental coast (Correa-Ramírez *et al.,* 2007). Mesoscale eddies are common structures in the south Pacific whose characteristics have been observed and described by satellite data (Hormazábal *et al.,* 2004; Chelton *et al.,* 2007) and information from drifters (Chaigneau & Pizarro, 2005). These structures can propagate westward at speeds similar to the theoretical propagation speed of Rossby waves and have similar sizes and characteristics. Because of the similarity in speed, size and surface structure, it is difficult to distinguish between eddies and waves from satellite data (Chelton & Schlax, 1996). However, the meridional deflection in the trajectory of the observed structures cannot be explained by wave theory, indicating that eddies are more predominant than Rossby waves in the mesoscale variability within the South Pacific ocean (Chaigneau & Pizarro, 2005; Chelton *et al.,* 2007).

In the southeastern Pacific, most mesoscale eddies observed by satellite altimetry come from the continental coast (Hormazábal *et al.,* 2004; Chaigneau & Pizarro, 2005, Chelton *et al.,* 2007), caused by baroclinic instabilities of coastal currents (Leth & Shaffer, 2001). Many of these eddies can reach oceanic islands and constitute an important mechanism that connects the island region with the continental coastal region (Andrade *et al.,* 2014). In addition to the horizontal transport of nutrients and heat, mesoscale eddies vertically transport nutrients, known as eddy pumping, which corresponds to one of the mechanisms associated with increased biological productivity in oceanic areas (Falkowski *et al.,* 1991; Aristegui *et al.,* 1997; McGillicuddy *et al.,* 2007). The interaction of mesoscale eddies with islands and seamounts adjacent to the EIP may support a significant fraction of the observed increases in phytoplankton biomass around this island region. The main goal of the present study is to characterize the temporal and spatial variability of

satellite Chl-*a* around the islands that make up the EIP, and discuss potential forcing mechanisms behind this variability.

MATERIALS AND METHODS

Study area

The EIP forms part of an extensive submarine ridge (~2800 km in length; Sepúlveda, 1987) in the southeastern Pacific Ocean, known as the "Easter Island Hot Line," which extends over ~27°S, from the Desventuradas Islands (San Félix Island and San Ambrosio Island) at its eastern most point to Easter Island at its western most point (Fig. 1). The EIP is comprised of two islands of volcanic origin, (1) Easter Island (EI; 27°09'S, 109°23'W), and (2) Salas y Gómez Island (SGI; 26°27'S, 105°28'W) which are separated by a distance of ~414 km. EI is located ~3700 km from the continent and has a triangular surface of ~173 km^2 and has a maximum elevation of 560 m, located at the summit of the Maúnga Terevaka volcano (González-Ferrán, 1987). Its coast has many cliffs and only three small sandy beaches (Anakena, La Perouse and Ovahe) (Fig. 1b). SGI, located east of EI, covers an area of 2.5 km^2 and has a maximum elevation of 30 m, near Punta López. It has a bi-lobed shape, with a lower and narrower central sector that remains covered by water during the high tide (Castilla & Oliva, 1987) (Fig. 1c).

Satellite information

Approximately ten years (2002-2012) of sea level, geostrophic currents, winds, Chl-*a*, and sea surface temperature from satellite data were used in order to characterize spatial and temporal variability of satellite Chl-*a* around the islands of the EIP. Weekly sea level and geostrophic current data with a spatial resolution of 25 km were obtained from the combined product of the Topex/Poseidon, ERS and Jason missions 1-2, distributed by AVISO (http://aviso.oceanobs.com). Daily wind data, with a spatial resolution of 25 km, were obtained from "Cross-Calibrated Multi-platform Ocean Surface Wind" (CCMP) which integrates measurements from SSM/I, SSMIS, AMSR-E, TRMM TMI, QuickScat, SeaWinds and WindSat missions (http://podaac.jpl.nasa.gov/). Daily Chl-*a* data (OC3 algorithm; Werdell, 2009) and sea surface temperature with a 4 km spatial resolution were obtained from level-3 products from the MODIS-Aqua mission (http://oceancolor.gsfc.nasa.gov/).

Data analysis

Gaps in satellite Chl-*a* and sea surface temperature due to cloud cover were filled through an objective interpo-
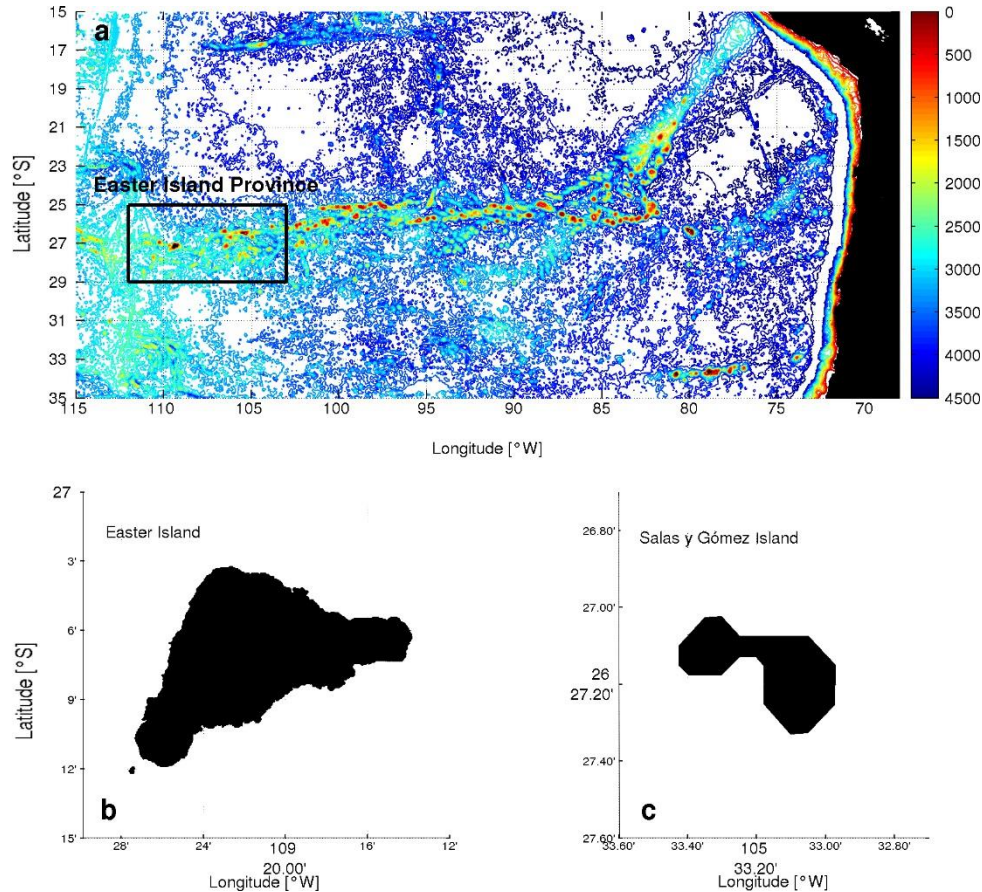
Figure 1. a) Geographic location of the Easter Island Province, b) Easter Island (27°09'S, 09°23'W), c) Salas y Gómez Island (26°27'S, 105°28'W).

lation using the DINEOF method (Data Interpolating Empirical Orthogonal Function) and applied iteratively through a mobile box of 31 days (Alvera-Azcárate *et al.,* 2007).

The analysis of the different variables was performed within a regional scale, which integrates the EIP in an area of nine degrees latitude (22°-31°S) and 15 degrees longitude (115°-100°W) (Figs. 2, 6, 10). In parallel, due to their higher spatial resolution (4 km), Chl-*a* and sea surface temperature databases were treated on a local scale, which considered the area around EI and SGI individually. For EI, a 1°x1° area (26.7-27.7°S, 109.8-108.8°W) was evaluated and for SGI, an area of 0.5°x0.5° (26.2-26.7°S, 105.7-105.2°W) (Figs. 3-9) was considered.

The spatial and temporal variability of main frequencies for different variables was evaluated using the "MultiTaper Method-Singular Value Decomposition" (MTM-SVD) method. This method allows the estimation of an average power spectrum for multiple time series distributed over a wide geographic region and the subsequent reconstruction of spatial fre-

quencies of interest (Mann & Park, 1999; Correa-Ramírez & Hormazábal, 2012).

RESULTS

Mean Easter Island Province conditions

Time averages of wind stress, wind stress curl, sea level, geostrophic currents, sea surface temperature and satellite Chl-*a* for the EIP are shown in Figure 2. In the study area wind stress (arrows; Fig. 2a) has a regular east to west direction with higher magnitudes (0.04-0.07 Nm^{-2}) to the north of the islands, and a regular east to southeast direction of lower magnitudes (0.01 to 0.03 Nm^{-2}) to the south of the islands. The surface wind generates a positive low-magnitude (0.4-0.5x10^{-7} Nm^{-3}) curl with greater intensity in the center of the south Pacific anticyclone, located southeast of the islands. The average sea level field shows that the islands are near the center of the subtropical gyre (Fig. 2b), identified by maximum sea level values to the northwest of the islands.
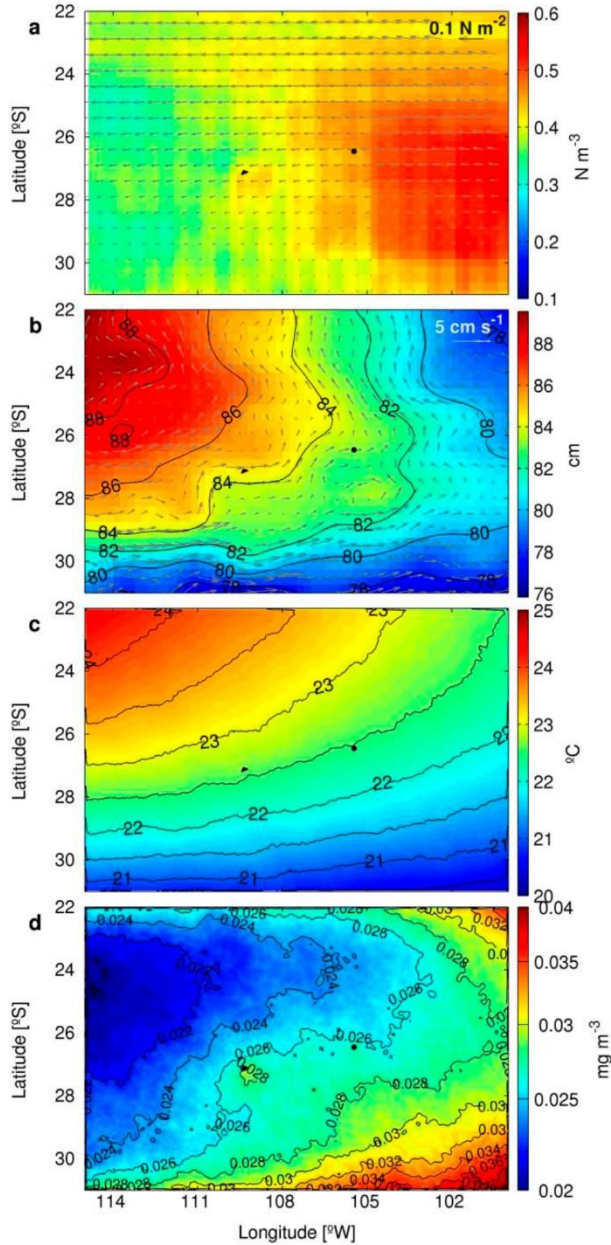
Figure 2. Temporal averages of a) wind stress (arrows; Nm^{-2}) and wind stress curl (Nm^{-3}), b) sea level (cm) and geostrophic currents (arrows, cm s^{-1}), c) sea surface temperature (°C), and d) satellite Chl-*a* (mg m^{-3}) within EIP. Eighteen years (1992-2011) of data available for the calculation of the averages of a) and b), and ten years (2002-2012) of data available for c) and (d) were used.

The temporal average of the geostrophic currents indicates a predominantly anticyclonic circulation (Fig. 2b). The mean sea level field shows that the islands are on the southern boundary of the South Pacific subtropical gyre, and are affected by the Subtropical Countercurrent (STCC), which flows to the east on 25°S between 150°-110°W (Moraga *et al.,* 2010). The

STCC changes its direction to the north after passing the island (Fuenzalida *et al.,* 2008).

At a regional scale, there is an interruption of the flows northeast from EI, which divides the main current in two when coming in contact with the island; a eastward flow at the southern side of the island and a recirculation flow (as an eddy) at the northern side of the island (Fig 2b). On the other hand, the characteristics of the temporal average circulation pattern resemble the average satellite Chl-*a* field (Fig. 2d). suggesting a relationship between the current and increases/decreases in phytoplankton biomass in these waters. The average field of satellite Chl-*a* exhibits very low concentrations (~0.029 mg m^{-3}) (Fig. 2d). A gradual decrease in average satellite Chl-*a* concentrations is observed from east (0.038 mg m^{-3}) to west (0.022 mg m^{-3}), with a slight increase towards the south of EI (0.028 mg m^{-3}). This pattern is opposite to those shown by the sea level (Fig. 2b) and sea surface temperature (Fig. 2c). Also, there is a local increase around EI that is represented at the temporal average. This Chl-*a* local increase will be discussed later at a local scale. On the other hand, at SGI, Chl-*a* local increases are not observed in the temporal average.

The average field of sea surface temperature is shown in Figure 2c. The temperature around the EIP increases gradually from the southeast (20.5°C) to the northwest (24°C) and the two islands are located near the isotherm of 22.5°C.

The mean field of satellite Chl-*a* and sea surface temperature for Easter Island (1°x1°) and Salas y Gómez Island (0.5°x0.5°) is shown in Figure 3. These mean fields were obtained from ten years of Chl-*a* and sea surface temperature data with a 4 km spatial resolution. On a local scale, a marked dipole in Chl-*a* concentrations is observed near EI (area: ~173 km^2), dividing the island in two regions; the southeast and the northwest (Fig. 3a). The southeast region presents higher mean Chl-*a* concentrations (0.029 mg m^{-3}) than the northwest (0.025 mg m^{-3}), whose values are within the range reported by Pizarro *et al.* (2006) for this island. For SGI the mean Chl-*a* values are about 0.027 mg m^{-3} (Fig. 3b). The SGI did not produce a significant effect on Chl-*a* concentrations due to its small size (2.5 km^2) and low elevation (30 m).

The mean sea surface temperature field shows surface temperature gradients of near 0.1°C at 20 km. Similar to the Chl-*a* fields, a temperature dipole is observed at EI which divides the island into southeastern and northwestern zones (Fig. 3c). The region of highest mean temperature (22.70°C), the northwest of EI, coincides with the lowest mean Chl-*a* values. While in the southeast the lowest temperature (22.55°C) and the highest Chl-*a* values were observed,
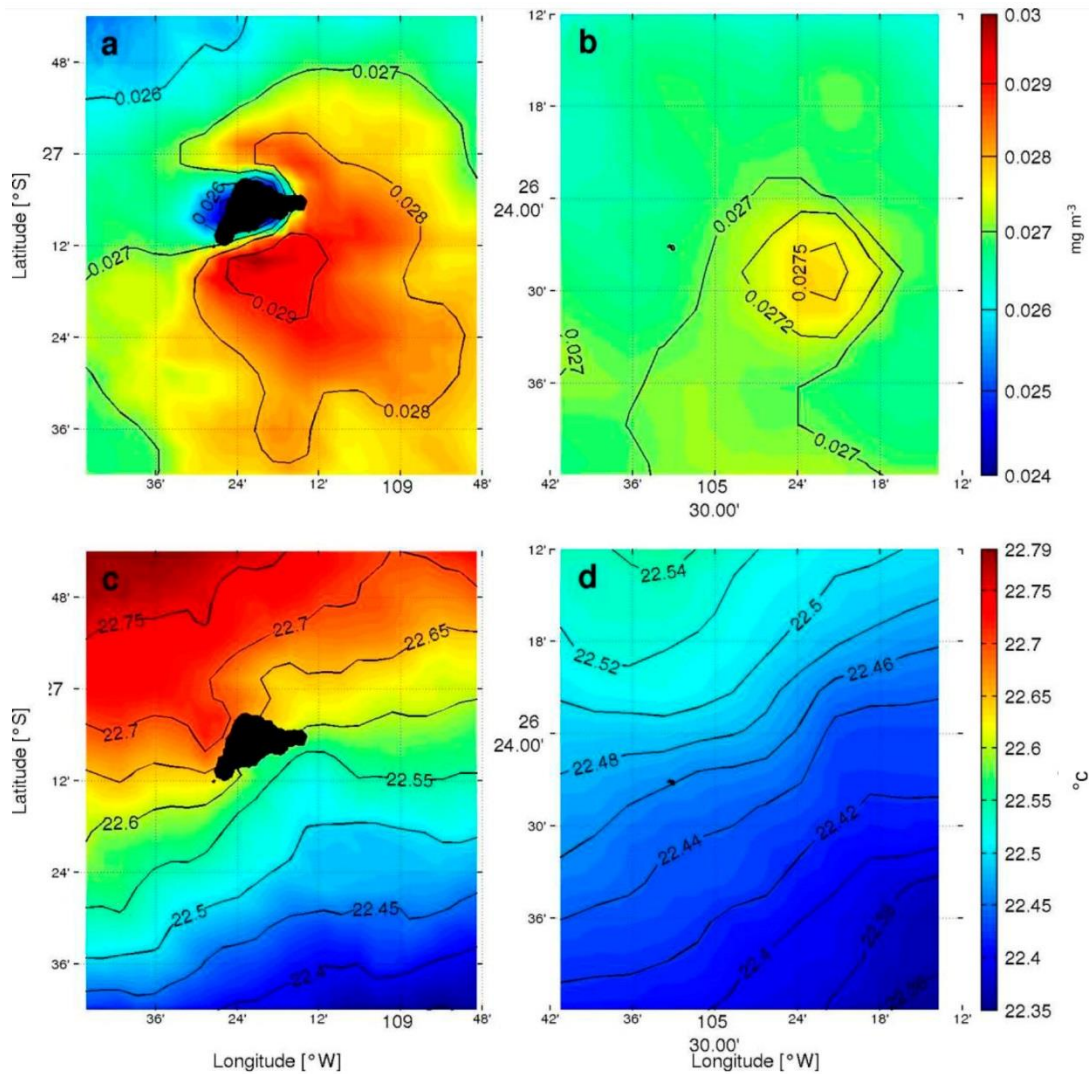
Figure 3. Temporal average of satellite Chl-*a* in mg m⁻³ and sea surface temperature in °C (contour lines) during the period 2002-2012 in a) and c) Easter Island, b) and d) Salas y Gómez Island, respectively.

indicating an inverse relationship between both variables. Furthermore, the SGI has slightly lower mean temperature values (22.46°C) than those observed for EI (Fig. 3d).

Variability scales

Spectra of local fractional variance (LFV) for satellite Chl-*a*, computed using the MTM-SVD method for EI and SGI, are shown in Figure 4. On both islands, the spectra LVF for Chl-*a* shows a significant peak (>99%) in a wide frequency band centered on annual (315-431 days) and semiannual (172-195 days) periods. Within the interannual band, SGI has greater variability with significant peaks with periods of 2.5 year (>99%), 1.7 year (>99%) and 7.5 year (>90%). Meanwhile, EI shows less variability within the interannual band, with one maximum at ~2.4 years (90%).

The spectra of LFV for satellite sea surface temperature around EI and SGI, calculated through the MTM-SVD method, is presented in Figure 5. For EI, sea surface temperature presented maximums (>99%) in a wide band centered on the annual period (309-455 days), as well as maximums (>80%) in the interannual (1.87 years) and semi-annual (174-195 days) bands (Fig. 5a). For SGI, the spectra of LFV also presented a significant maximum (>99%) over a wide frequency band centered on the annual cycle (303-455 days). Sea surface temperature variability also contributed significantly (>95%) to the semiannual (174-195 days) and interannual (3 and 2.2 years) bands, and with a lesser degree of significance (>90%) in ~4.5 years and 1.4-1.6 years (Fig. 5b).

The time scales of variability for sea level and geostrophic current were computed using the MTM-
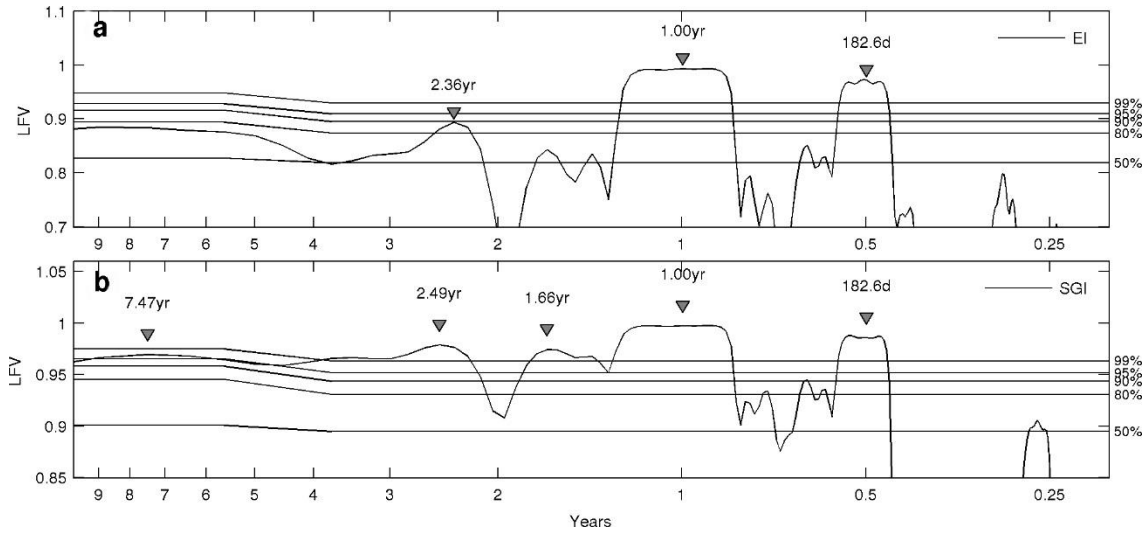
Figure 4. Spectra of local fractional variance (LFV) on times scales ~10 years for satellite Chl-*a* a) for Easter Island (EI; 26.7-27.7ºS, 109.8-108.8ºW), and b) Salas y Gómez Island (SGI; 26.2-26.7ºS, 105.7-105.2ºW). Confidence levels of 50, 80, 90, 95 and 99%, were calculated through a bootstrap resampling.
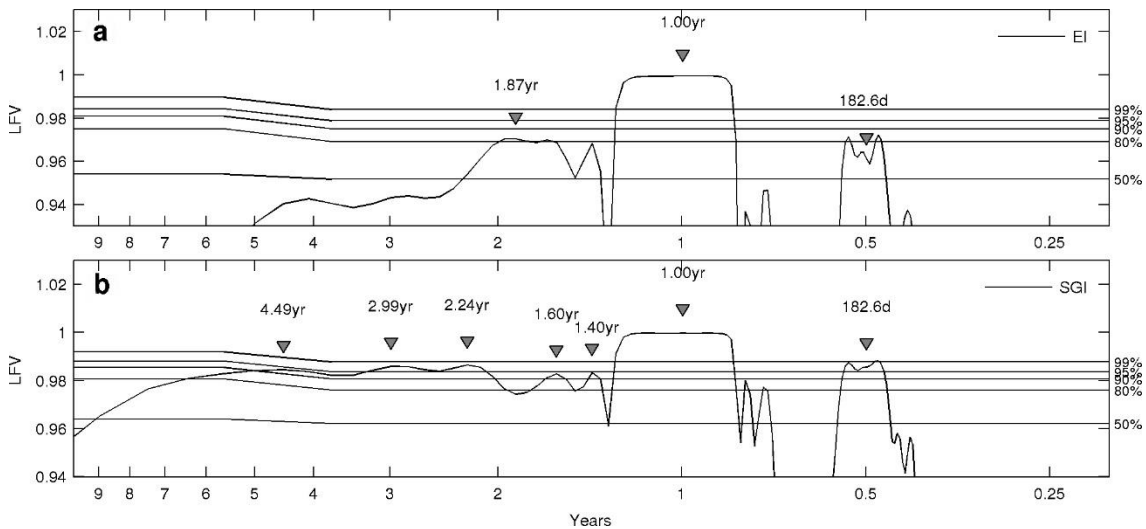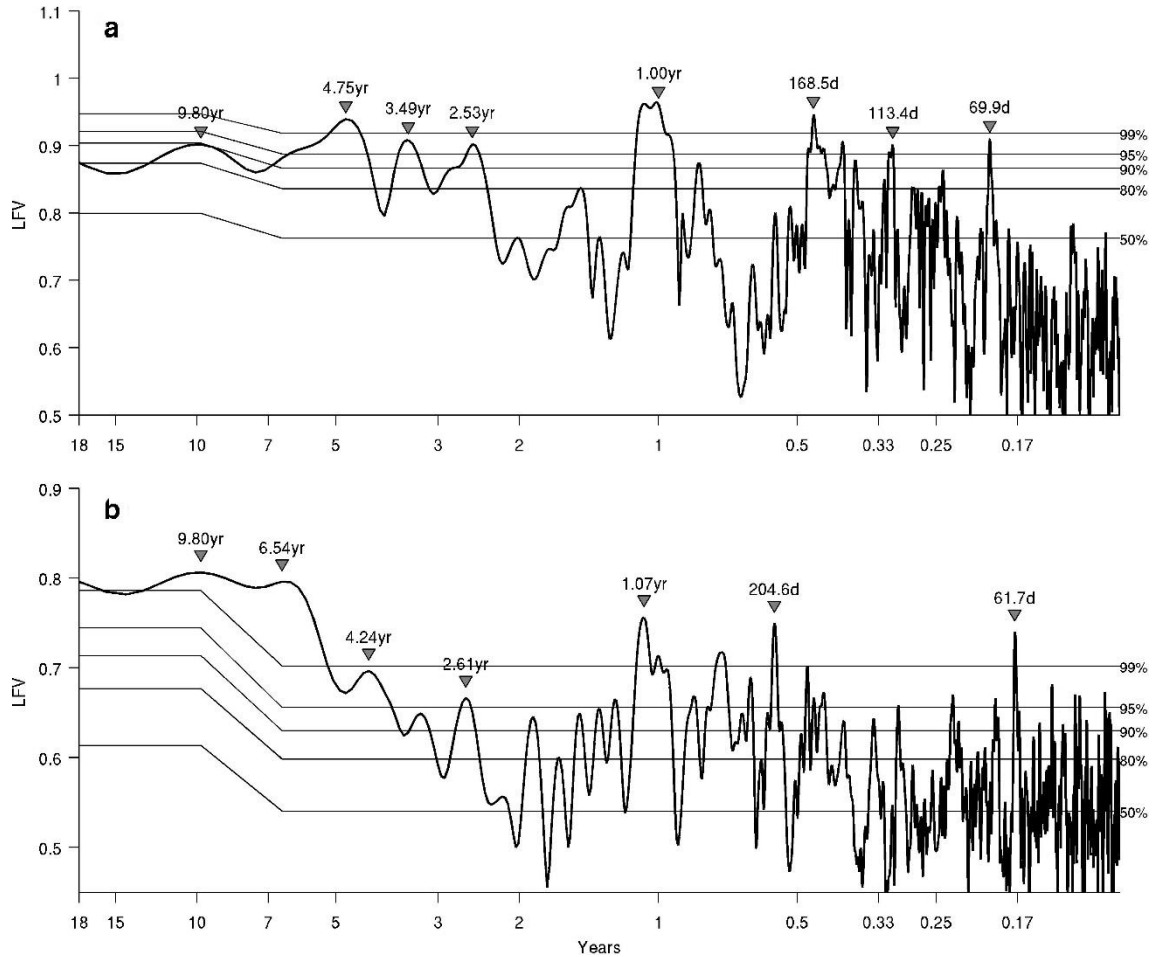

Figure 5. Spectra of local fractional variance (LFV) on times scales of ~10 years for satellite sea surface temperature around a) Easter Island (EI; 26.7-27.7ºS, 109.8-108.8ºW), and b) Salas y Gómez Island (SGI; 26.2-26.7ºS, 105.7-105.2ºW). Confidence levels of 50, 80, 90, 95 and 99% were calculated from bootstrap resampling.

SVD method and are shown in Figure 6. In the sea level spectrum (Fig. 6a), the largest fraction of variability is observed in the annual frequency (>99%). In the interannual band, the LFV spectra for both variables showed significant peaks (>95%) for periods of 9.8 years, ~4 years and ~2.5 years (Figs. 6a-6b). Additionally, geostrophic currents within the interannual band have a maximum at ~6.5 years (>99%), which is not observed in the sea level spectrum. Both the sea level and the geostrophic current spectrum exhibit significant maximums (>99%) on semiannual (~180 days) and intraseasonal (~65 days)

bands. In particular, the high intraseasonal variability observed in the area could be linked to the persistent presence of mesoscale structures (Hormazábal *et al.,* 2004) or the effect of atmospheric forcing within the region (Hormazábal *et al.,* 2001, 2002).

Annual cycle of chlorophyll-*a*

Annual satellite chlorophyll-*a* and sea surface temperature cycles for EI and SIG are shown in Figure 7. On both islands, Chl-*a* shows a marked annual cycle with higher concentrations (~0.051 mg m^{-3}) in austral winter, centered on July (Fig. 7a), consistent with what

Figure 6. Spectra of local fractional variance (LFV) on times scales ~18 years for a) sea level, and b) geostrophic currents within EIP (2-32ºS, 115-100ºW). Confidence levels of 50%, 80%, 90%, 95% and 99% were calculated by from bootstrap resampling.
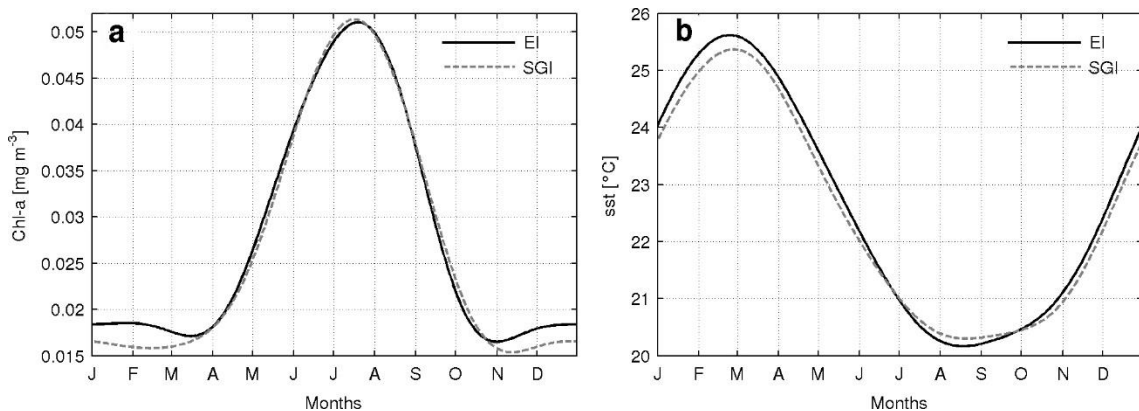
Figure 7. a) Annual satellite Chl-*a* cycle, and b) sea surface temperature for Easter Island (EI; 26.7-27.7ºS, 109.8-108.8ºW) and Salas y Gómez Island (SGI; 26.7-27.7ºS, 109.8-108.8ºW), obtained by harmonic analysis over the 2002-2012 period.

has been described by other authors for the oceanic region off Chile (Yuras *et al.,* 2005; Correa-Ramírez *et al.,* 2007; Andrade *et al.*, 2012.). For EI, Chl-*a*

maximums during winter begin to decline towards the end of July, reaching its lowest value (0.017 mg m⁻³) in late October-early November. After reaching its mini-
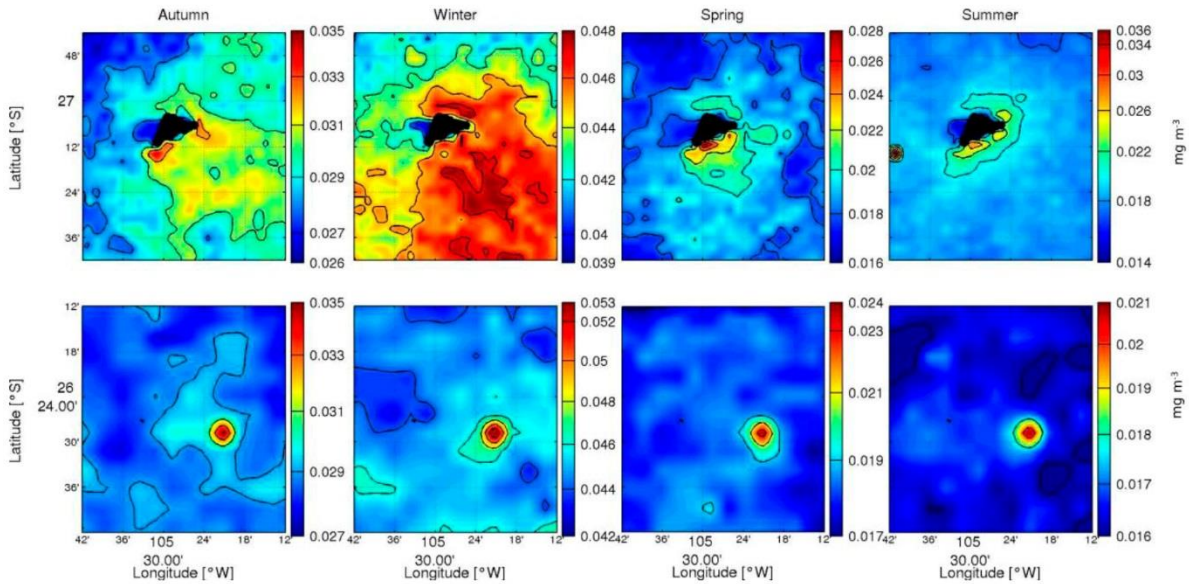
Figure 8. Seasonal cycle of satellite Chl-*a* (mg m^{-3}) for Easter Island (upper panels) and Salas y Gómez Island (lower panels). As the range of variability of Chl-*a* concentrations are low , different color bars for each panel are used, therefore the color representation of each graph is not comparable directly.
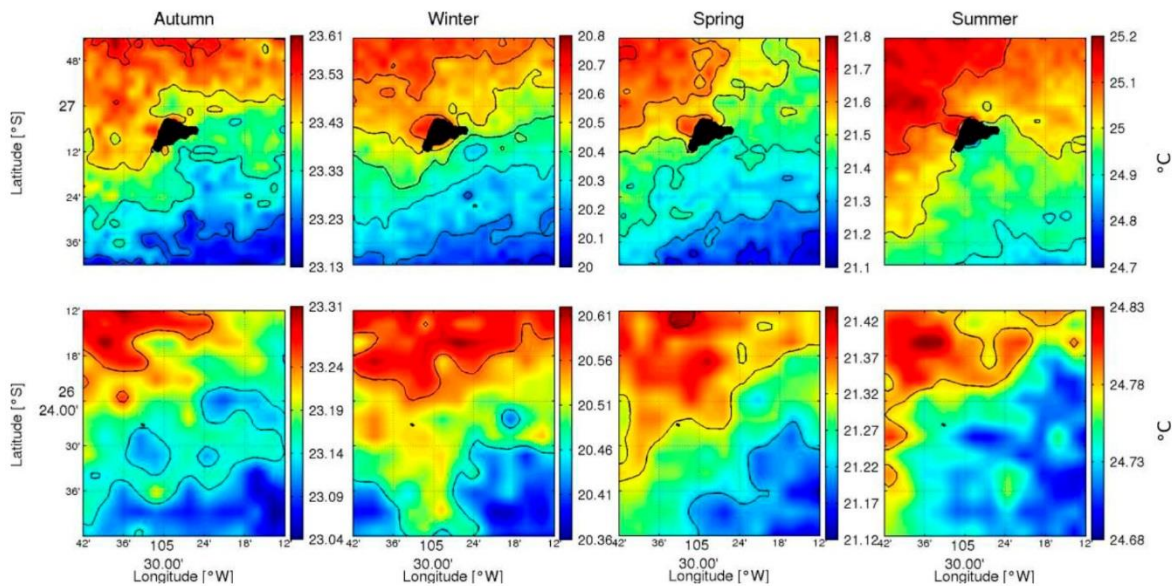
Figure 9. Seasonal cycle of satellite sea surface temperatures (°C) for Easter Island (upper panels) and Salas y Gómez Island (lower panels). As the temperature ranges are low, different color bars are used for each panel, therefore, the color representation of each graph is not comparable directly.

mum, a slight increase occurred reaching a maximum in summer (~0.019 mg m^{-3}) in late December-early January, ending with low concen-trations in late March (0.017 mg m^{-3}). For SGI, the annual Chl-*a* cycle showed a similar pattern to that seen for EI, the winter maximum had a similar amplitude, however the second increment in Chl-*a* observed in summer had an amplitude similar to minimum values recorded for EI (Fig. 7a).

The annual satellite sea surface temperature cycle for both islands showed a marked annual cycle, with higher (lower) temperature values during the summer (winter) period (Fig. 7b). For EI, the summer maximum (25.62°C) is reached in late February-early March, and

a minimum (20.17°C) reached in mid August. For SGI, the annual sea surface temperature cycle showed a similar pattern to that seen at EI, recording its maximum value (25.37°C) in late February and its minimum value (20.31°C) in mid August (Fig. 7b).

The Chl-*a* satellite seasonal cycle around EI and SGI is shown in Figure 8. As variations in Chl-*a* concentrations are low, a different color bar for each figure is used. Overall, both study areas had the highest Chl-*a* concentrations during the winter period, with the highest values (0.053 mg m^{-3}) in SGI. For EI, the Chl-*a* fields for autumn (0.035 mg m^{-3}) and winter (0.048 mg m^{-3}) periods exhibited a regional extension, however the highest concentrations were southeast of the island (~2 km). During spring, the lowest Chl-*a* concentrations (0.028 mg m^{-3}) were observed. At this time, the spatial extension of the highest Chl-*a* concentrations began to reduce, focusing the highest Chl-*a* concentrations toward the south-southeast of the island and showing an IME. This IME reached its maximum expression in summer, when the extension of the highest Chl-*a* values was further reduced on the southeast side of the island. Furthermore, it can be seen that average Chl-*a* fields formed a dipole around EI that remains throughout the year. This dipole separated the island into two zones; a northwest area with the lowest Chl-*a* concentrations within the region and a southeast area with highest concentrations. For SGI, increases were concentrated toward the Southeast of the island, with the highest concentrations occurring during winter (0.053 mg m^{-3}) and the lowest concentrations during summer (0.021 mg m^{-3}). Here, the bloom of Chl-*a* was located on an extensive platform associated with a seamount located ~2 km to the east of the island whose summit is ~50 m below the sea surface.

The seasonal cycle of satellite sea surface temperature around EI and SGI is shown in Figure 9. The seasonal variation was ~5°C but the spatial ranges of temperature variation (<1°C) within each season are small, so a separate color bar for each panel was used. Overall, both islands had the highest temperature values during the summer period and EI had higher temperatures (25.2°C) than SGI (24.8°C). On both islands a gradual increase in temperature was observed from the southeast to the northwest of the region. However, on the northwest side of EI a permanent local increase in temperature that is more intense during winter and spring was observed. This local increase seems to coincide with a permanent zone of low chlorophyll concentrations observed in Figure 8.

Mesoscale eddies

The sea level and surface current fields in the region shows a high variability generated by the persistent passage of mesoscale eddies, as observed in the sequence presented in Figure 10 (a-h, arrows). The figure shows a typical trajectory of two mesoscale eddies; a cyclonic eddy (C1) and an anticyclonic eddy (A1), for a period of ~7 months (April 18-October 29, 2012) covering an autumn, winter and spring period. On April 2012, the C1 eddy interacted with the south coast of SGI and Chl-*a* concentrations increased within the eddy in May, 2012 (Figs. 10a-10b). A month later (June 2012), the C1 eddy moved westward and lost contact with the SGI; however; the A1 eddy began interacting with SGI. This structure also generated an increase of Chl-*a* concentrations upon entering in contact with the island in July 2012 (Figs. 10c-10d). During this month, the C1 eddy reached the east coast of EI and continued its movement around the southern flank of the island during August 2012 (Figs. 10d-10e). In September 2012, the C1 eddy separated from EI and reached the A1 eddy, which remained on the southern coast of the island until October 2012 (Figs. 10f, 10h).

In the Chl-*a* fields shown in Figure 10 (a-h; color), the regional extension of Chl-*a* concentrations and their relation to the presence of mesoscale eddies can be observed. The Chl-*a* concentrations associated with the borders and center of eddies reached up to ~0.1 mg m^{-3} during winter, (Figs. 10d, 10f) which represents two orders of magnitude higher than common concentrations in subtropical gyre waters (~0.001 mg m^{-3}). The regional extension of Chl-*a* fields covered the entire EIP between late autumn and mid-winter (Figs. 10c, 10f). As of October a retreat to the southeast of Chl-*a* fields can begin to be observed, with maximums during the spring-summer periods. As will be described in detail in the next section, during this latter period, which corresponds to the seasonal Chl-*a* minimum in the region (Fig. 7), around EI the Chl-*a* showed local increments on a submesoscale level associated with the perturbation of oceanic flow caused by the presence of the island.

Submesoscale eddies

During the autumn-winter seasons, Chl-*a* fields showed regional increases in concentrations as a mean condition of their annual cycle. During spring-summer periods, the Chl-*a* fields were restricted to the EI coast (Figs. 8, 10).

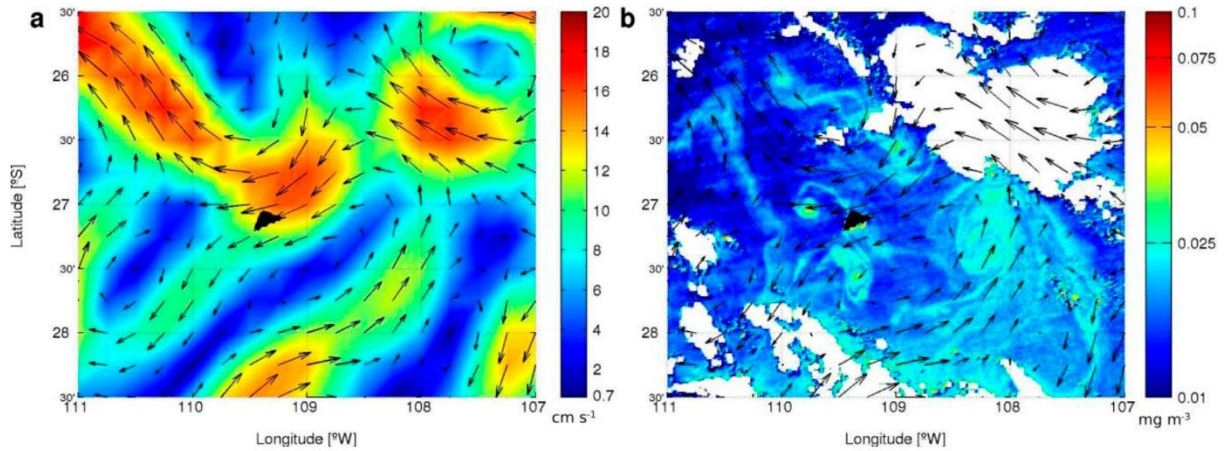Figure 11 shows the current field (arrows), superimposed onto the current magnitude field and on the Chl-*a* field surrounding EI for October 29, 2012. The Chl-*a* satellite field with a 1x1 km spatial resolution showed Chl-*a* wake formations associated with the detachment of submesoscale eddies from EI (Fig. 11b). Chl-*a* concentrations within the wakes had maximum values (~0.1 mg m^{-3}) along the northwest and southeast coast
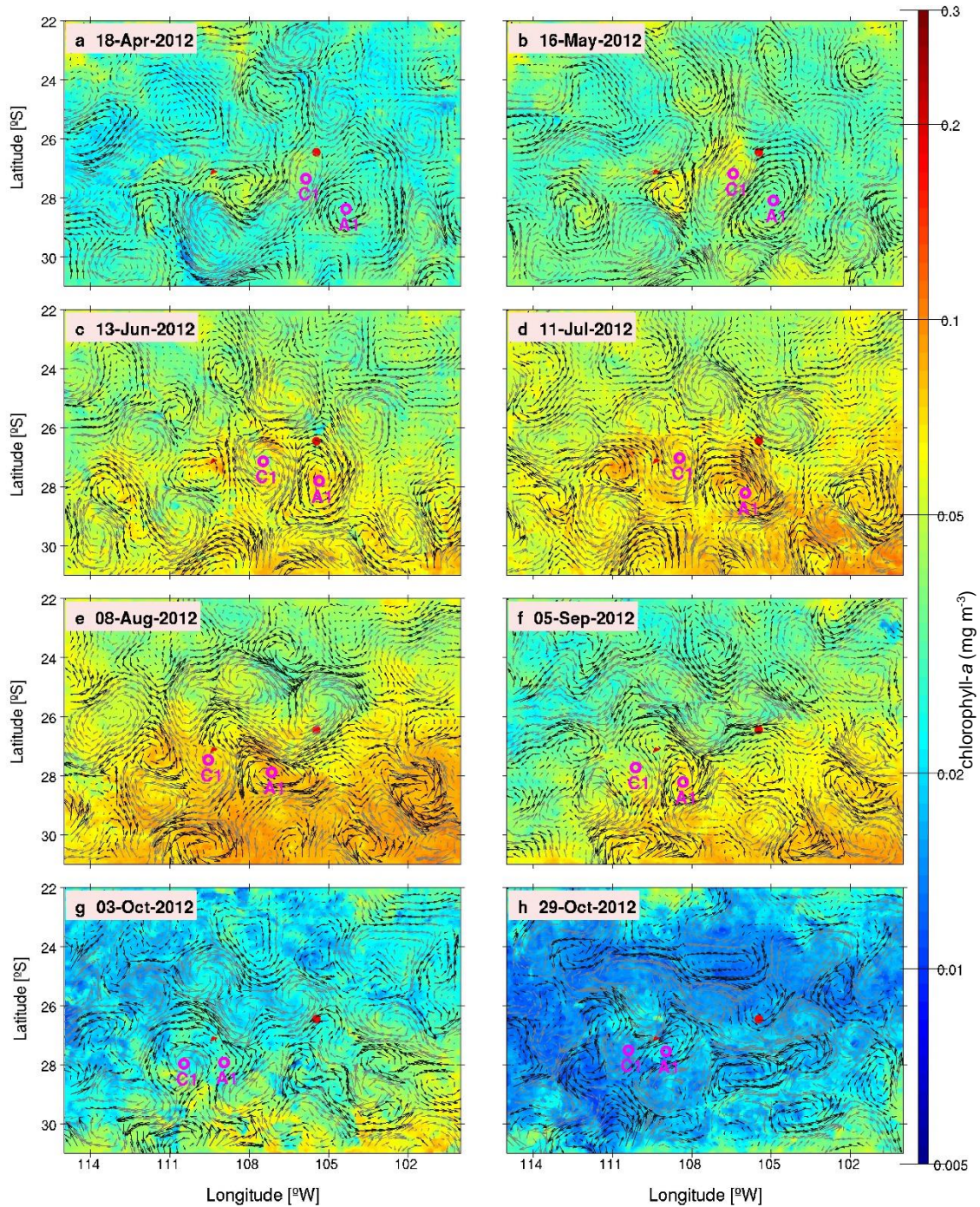
Figure 10. Geostrophic current surface field in m s^{-1} (arrows) superimposed on Chl-*a* fields in mg m^{-3} (colors) for selected periods between April 18 and October 29, 2012. The magenta circles indicate the position of the displacement of two eddies: cyclone (C1) and anticyclonic (A1), which propagate westward passing close to both islands. The red marks indicate the position of Easter Island and Salas y Gómez Island.

of the island, representing two orders of magnitude higher than adjacent oceanic waters (~0.001 mg m^{-3}). From the increments on the northwestern side, a Chl-*a* wake can be observed ~50 km long that connected to an eddy at the far end with similar dimensions as those

of the island. Chl-*a* wakes can also be observed on the western side of the island that were connected to two submesoscale eddies with clear increases in Chl-*a* at their centers.

Figure 11. Current field (arrows), superimposed a) on the current magnitude field and b) on the Chl-*a* field around Easter Island for October 29, 2012. Chl-*a* (mg m^{-3}) shows the presence of submesoscale eddies to the south and north of the island. The chlorophyll-*a* data has a spatial resolution of 1 km and the current data 25 km.

The current field surrounding EI showed the presence of cyclonic and anticyclonic mesoscale eddies, where the contact area between mesoscale eddies had the largest current magnitude (Fig. 11a). Furthermore, it can be observed that EI was exposed to the contact zone between a cyclonic eddy located north of the island and an anticyclonic eddy located to the south of the island, with current magnitudes of 10-14 cm s^{-1} (Fig. 11a).

According to theoretical studies conducted in laboratory experiments and numerical simulations (*e.g.,* Gerrad, 1978; Heywood *et al.,* 1996; Barton, 2001; Dong *et al.,* 2007), a submesoscale eddy street is formed when the incident flow is sufficiently energetic so that the Reynolds number (Ree) that represents the ratio between non-linear parameters and viscosity is >80. Ree is defined as:

$$Ree = \frac{UL}{V_e}$$

Where U, is the incident flow velocity, L is the diameter (~24 km for EI), and v_e is the eddy viscosity coefficient. In the ocean v_e increases with the length of the scale of interest in the following form: $v_e = 2.2 \times 10^{-4} L^{1.13}$ (Barton, 2001). Thus, for EI v_e is 19.6 m^2 s^{-1}. Ree values = 100 are considered necessary in order for an eddy streets to be produced, an incident flow velocity of >8.2 cm s^{-1} is needed which, as seen in Figure 11a, is achieved due to the incident flow rate EI having values of between 10 and 14 cm s^{-1}. Due to the slow displacement of mesoscale eddies (~2 km d^{-1}; Hormazábal *et al.,* 2004), the flow incident can persist

during at least one week and allow the submesoscale vortices formation.

The westerly component of Chl-*a* wakes can be seen in Figure 11b. As mentioned in section 3.4, the mean flow direction around the EIP is predominantly westward due to the propagation of mesoscale eddies, which have a higher mean speed than the mean geostrophic flow heading east. This suggests that mesoscale variability could be fulfilling an important role in the formation of submesoscale eddies around these oceanic islands. Moreover, the contact zones between mesoscale eddies seems to intensify the incident flow on the islands, and promotes the formation and detachment of submesoscale eddies and filaments associated with high Chl-*a* concentrations.

DISCUSSION

EIP is the most westerly territory of Chile, located near to center of the south Pacific subtropical gyre, which determine the major characteristics of the circulation around these islands. The location of the subtropical gyre center is determined by the combined effect of wind and buoyancy and it does not coincides geographically with the location of the south Pacific anticyclone's center (McClain *et al.,* 2004). In effect, the EIP is located approximately equidistant between the center of the subtropical gyre's rotation and the south Pacific anticyclone. The position of the centers of these two systems (subtropical gyre and south Pacific anticyclone) have a seasonal and interannual variability related to El Niño and the Southern Oscillation (Correa-Ramírez & Hormazábal, 2012).

The magnitude and direction of the geostrophic currents in EIP are consistent with currents observed by Moraga *et al.* (2010), at 5 m and 30 m depths, registering average magnitudes of 6.2 and 8.2 cm s^{-1}, respectively. Part of the spatial variability observed in the average sea level and current fields in the region appear to be determined by island topography and seamounts that make up the "Easter Island Hot Line" (González-Ferrán, 1987), generating a quasi-permanent meander around EI and, additionally, some eddies observed south of SGI (Fig. 2b). At a local scale, Moraga *et al.* (2010) suggest that the flows could be modified in the vicinity of EI (on a ~10 km scale), showing differences with the geostrophic circulation defined by hydrographic data. This effect cannot be perceived at distances greater than ~10 km from the island, where the circulation associated with the south Pacific anticyclonic gyre dominates (Moraga *et al.*, 2010).

The overall characteristics of the temporal average circulation pattern are resemble the average satellite Chl-*a* field, showing high (low) Chl-*a* concentrations associated to low (high) sea level values. This suggest a relationship between the current and increases/decreases in phytoplankton biomass in region. Unfortunately, local circulation patterns and their influence on the distribution of nutrients, primary productivity and fish aggregations have not yet been evaluated within this region.

The southeast-northwest temperature gradient observed in EIP, has been associated with the effect of the interaction between water masses that are transported by the STCC and the oceanic branch of the Humboldt Current System, which transports Subantarctic Surface Water to north of the subtropical gyre (Fuenzalida *et al.*, 2008). Furthermore, these authors suggest that a significant portion of sea surface temperature variability in this region could be linked to the seasonal variability of the Humboldt Current's position and intensity.

The low concentrations (~0.029 mg m^{-3}) observed in EIP (Fig. 2d), are two orders of magnitude lower than concentrations found off the continental coast (on average ~10 mg m^{-3}; ~71°W; Yuras *et al.*, 2005) and one order of magnitude lower than the concentrations observed in the coastal region of the Juan Fernández Archipelago (on average ~0.4-0.5 mg m^{-3}; ~81-79°W; Pizarro *et al.*, 2006; Andrade *et al.*, 2012). Because the low Chl-*a* concentrations, these waters has been recognized like the most transparent in the world (Pizarro *et al.*, 2006). The slight increase towards the south of EI (0.028 mg m^{-3}), suggest that the island has a localized effect on Chl-*a* concentrations, which is represented in the average fields.

The small dimensions of SGI (2.5 km^2) and the low resolution of the satellite data used does not allows observe local increases in Chl-*a* concentrations around this island. However, towards the southeast of SGI a slight increase of Chl-*a* (~0.0005 mg m^{-3}) is observed, which could be associated with seamounts in the region. SGI is part of a large submarine volcano, 3,500 m high, which has an additional peak located ~2 km southeast of SGI that rises to ~50 m below the ocean surface (González-Ferrán, 1987). This summit has an extensive platform to the east, whose depths reach the euphotic layer (not shown). It is likely that the ocean and atmosphere's interaction with this platform may support the suspension of nutrients and generate the Chl-*a* nucleus (0.0275 mg m^{-3}) observed southeast of the island (Fig. 3b).

The variability of the Chl-*a* and sea surface temperature in the EIP have a strong annual cycle. However, several frequencies of variability were also observed within the interannual band (periods of ~7.5, 4.5, 3, 2.5 years) mainly in the sea surface temperature. These frequencies have generally been associated with disturbances caused by El Niño and the Southern Oscillation in the southeastern Pacific (Correa-Ramírez *et al.*, 2012). Despite the short distance between EI and SGI (~414 km), only SGI showed a larger number of frequencies with major energy associated to the interannual band, what could suggest that both islands are exposed to development of different oceanographic dynamics.

The seasonal maximum of Chl-*a* in the south Pacific subtropical gyre occur in winter, when the mixing layer is deep and the depth of the isoline, at 2 μM, are relatively shallow, causing phytoplankton to produce more Chl-*a* as a photo-adaptive response to lower light levels imposed by deeper mixing (Winn *et al.*, 1995; McClain *et al.*, 2004). It has been suggested that during the winter, this biological strategy is more important than the vertical mixing of nutrients, as the nutricline at this time is deeper than the mixed layer (McClain *et al.*, 2004).

The low changes along the year in Chl-*a* concentrations observed around the EI and SGI are an important biological characteristic in the subtropical gyres. However, a great variability in phytoplankton growth rates associated to minimal changes in phytoplankton biomass has been observed in the subtropical gyres (McClain *et al.*, 2004). Therefore, the low seasonal changes in Chl-*a* around EI and SGI could have deep and unknowed impacts in the island marine ecosystems.

As the Chl-*a* and sea surface temperature, the largest fraction of variability in the sea level and geostrophic currents are in the annual and the interannual bands. For

the southeastern Pacific, it has been documented that the annual sea level cycle is dominated by Rossby wave propagation from the continental coastline (Correa-Ramírez *et al.,* 2012). This annual Rossby wave propagation could modify the intensity and position of currents within the region, mainly the STCC and the Humboldt Current System (Fuenzalida *et al.,* 2008).

Although the average current flow in EIP was dominated by the STCC, the sea level and surface current fields in the region are characterized by high variability generated by the persistent passage of mesoscale eddies (Fig. 10). These structures cross the island region during their displacement towards the west, with a mean speed of ~2 km d^{-1} (Hormazábal *et al.,* 2004). A significant fraction of the long life eddies have been found between the coast and 100°W. These eddies originate in the continental coastal zone (Chaigneau *et al.,* 2005, 2009), and are possibly associated to baroclinic coastal current instabilities (Leth & Shaffer, 2001). Considering the average speed of mesoscale eddies, and assuming that they originate in the continental coastal zone, eddies with life spans longer than five years could reach EIP. However, the fraction of long life eddies in the EIP could be smaller since the generation of some these eddies has been observed in closer areas. The origin of mesoscale eddies arriving in the region and their impact on the transport of heat, nutrients and organisms are issues that have not been assessed in the EIP.

Despite the mean zonal current in EIP is towards the East, there are a significant temporal variability in the currents with periods of westward flow that appears in association with the passage of mesoscale eddies (Fig. 10). Since the mean speed of mesoscale eddies (~2 km d^{-1}) is greater than the mean zonal flow (~0.92 km d^{-1}) it is possible that these structures dominate the mean transport and the flow westward. In this sense, the transport associated with eddies could have deep implications for the connectivity of biological communities between islands and mainland areas. Because mesoscale eddies maintain many water properties associated to their formation area (Nauw *et al.,* 2006), the extended periods of permanency for mesoscale eddies in the EIP, and their interaction with both islands, could favor biological connectivity as well as egg and larvae retention, as has been observed in other islands (*e.g.,* Porovic *et al.,* 2012).

During spring-summer periods when the seasonal minima of Chl-*a* occur in the EIP, the Chl-*a* concentrations close to the insular coast remain higher than adjacent waters, which have been classically defined as Island Mass Effect (IME; Doty & Ogury, 1956). Our results shows that the submesoscale eddies formation is the main process behind the IME around

EI (Fig. 11). The formation of submesoscale eddies by islands is one of the most studied mechanisms related to oceanic islands (Heywood *et al.,* 1990, 1996; Sangrà *et al.,* 2007; Hasegawa *et al.,* 2009). The formation and subsequent detachment of these structures from the islands stimulate the vertical ascent of nutrients up to the euphotic zone, promoting phytoplankton bloom and/or the passive advection of subsurface phytoplankton maximums towards the surface (Hasegawa *et al.,* 2009).

The submesoscale eddies formation result in Chl-*a* wakes with high concentrations (~0.1 mg m^{-3}) in the eddies centers and low Chl-*a* concentration zones that connect them. The formation time of these structures is consistent with that previously reported for the Juan Fernández Archipelago (Andrade *et al.,* 2014), where IME develops with greater intensity in spring-summer.

Because mesoscale eddies have a higher speeds than the mean geostrophic flow, the mesoscale variability could be playing an important role in the formation of submesoscale eddies around these oceanic islands. Our results shows that contact zones between mesoscale eddies would intensify the incident flow on the islands, and promote the formation and detachment of submesoscale eddies and filaments associated with high Chl-*a* concentrations. The local formation of these structures may play an important role in the biological production around EI on a regional scale, especially during periods of low Chl-*a* concentrations.

CONCLUSIONS

EIP oceanic islands are located between the center of the anticyclonic winds and the center of the south Pacific subtropical gyre in an ocean area characterized by high temperatures and very low Chl-*a* concentrations, where the predominant current flows in an eastward direction and are determined by the influence of the Subtropical Countercurrent. Mean temperature and Chl-*a* distribution shows that the EIP is located within a regional gradient with a northeast-southwest direction, where the Chl-*a* (temperature) increases towards the southeast (northwest) in a way that approximates the subtropical front (subtropical gyre center). In this region, the annual cycle dominates oceanographic variability and is determined by seasonal change in the position of the main of currents and wind systems that affect the region.

The annual Chl-*a* cycle around the EIP presented maximum concentrations during winter period, which may be linked to an effect of phytoplankton photo-adaptation in response to the deepening of the mixed layer in winter and the remote contribution of nutrients by mesoscale eddies. The seasonal Chl-*a* distribution

and sea surface temperature around the coasts of EI and SGI are different from the regional distribution, which could be linked to local processes associated with the islands. EI shows a marked dipole in Chl-*a* concentrations and temperature, where the southeastern zone presents the highest mean Chl-*a* concentrations and lowest temperature, while the northwest has lower Chl-*a* concentrations and higher temperatures. Meanwhile, SGI, due to its small size and low altitude, generates a minor local effect on Chl-*a* concentrations but with significant increases in Chl-*a* ~2 km to the southeast, which could be associated with a seamount whose summit is found ~50 m below the surface, and which also has a platform in the same direction (Fig. 3b). Increases and changes in the distribution of Chl-*a* concentrations seen around the islands may be promoting the generation of areas suitable for the development of larval stages or high food concentrations for pelagic species.

For the EIP, Chl-*a* variability has significant fluctuations in the interannual band, which has generally been associated with disturbances generated by El Niño and the Southern Oscillation (Correa-Ramírez *et al.,* 2012); however; the physical mechanism through which this signal reaches the EIP are unknown. Only the SGI presents a significant contribution to the interannual sea surface temperature variability, which may be causing various oceanographic dynamics between these islands.

Due to the subtropical gyre, the mean current field in the EIP is to the east, favoring the transportation of waters from EI to SGI. However, the EIP is affected by the frequent passage of mesoscale eddies. Many of these eddies are generated at the continental border and move westward with speeds greater than the average flow of the region, generating a westward transport which could be an important mechanism for promoting a connectivity from SGI to the EI.

On a smaller scale, the formation of submesoscale eddies around EI was observed during spring, which could be associated with a strong incident flow produced in the contact area between mesoscale eddies. The submesoscale structures have similar sizes to the island and their Chl-*a* concentrations are several times higher than in adjacent oceanic waters (~0.001 mg m^{-3}). The formation of these structures could be essential for supporting biological activity during the spring-summer periods when minimal Chl-*a* concentrations are observed in this region.

ACKNOWLEDGMENTS

REFERENCES

Alvera-Azcárate, A., A. Barth, J.M. Beckers & R.H. Weisberg. 2007. Multivariate reconstruction of missing data in sea surface temperature, chlorophyll, and wind satellite fields. J. Geophys. Res-Oce, 112, C03008, doi:10.1029/2006JC003660

Andrade, I., S.E. Hormazábal & M.A. Correa-Ramírez. 2012. Ciclo anual de la clorofila-*a* satelital en el archipiélago de Juan Fernández (33°S). Lat. Am. J. Aquat. Res., 40(3): 657-667.

Andrade, I., P. Sangrà, S.E. Hormazábal & M.A. Correa-Ramírez. 2014. Island mass effect in the Juan Fernández Archipelago (33°S), southeastern Pacific. Deep-Sea Res. I, 84: 86-99.

Aristegui, J., P. Tett, A. Hernandez-Guerra, G. Basterretxea, M.F. Montero, K Wild, P. Sangra, S. Hernández-León, M. Canton, J.A. Garcia-Braun, M. Pacheco & E.D. Barton. 1997. The influence of island-generated eddies on chlorophyll distribution: a study of mesoscale variation around Gran Canaria. Deep-Sea Res. I, 44(1): 71-96.

Barton, E.D. 2001. Island Wakes. In: J. Steele, S. Thorpe & K. Turekian (eds.). Turbulence and diffusion. Encyclopedia of Ocean Sciences, Academic Press, pp. 1397-1403.

Castilla, J.C. & D. Oliva. 1987. Islas oceánicas chilenas: aspectos descriptivos y potencialidades. En: J.C. Castilla (ed.). Islas oceánicas chilenas: conocimiento científico y necesidades de investigaciones. Ediciones Universidad Católica de Chile, Santiago. pp. 15-35.

Chaigneau, A. & O. Pizarro. 2005. Surface circulation and fronts of the South Pacific Ocean, east of 120°W. Geophys. Res. Lett., 32, L08605, doi:10.1029/2004 GL022070

Chaigneau, A., G. Eldin & B. Dewitte. 2009. Eddy activity in the four major upwelling systems from satellite altimetry (1992-2007). Prog. Oceanogr., 83(1-4): 117-123.

Chelton, D.B. & M.G. Schlax. 1996. Global observations of oceanic Rossby waves. Science, 272(5259): 234-238.

Chelton, D.B., M.G. Schlax, R.M. Samelson & R.A. de Szoeke. 2007. Global observations of large oceanic eddies. Geophys. Res. Lett., 34(15): 1-5, doi:10.1029/2007GL030812.

Correa-Ramírez, M. & S. Hormazábal. 2012. MultiTaper method-singular value decomposition (MTM-SVD): variabilidad espacio-frecuencia de las fluctuaciones del nivel del mar en el Pacífico Suroriental. Lat. Am. J. Aquat. Res., 40(4): 1039-1060.

Correa-Ramírez, M.A., S.E. Hormazábal & G. Yuras. 2007. Mesoscale eddies and high chlorophyll concentrations off Central Chile (29°-39°S). Geophys. Res. Lett., 34, L12604, doi:10.1029/2007GL029541.

Correa-Ramírez, M.A, S.E. Hormazábal & C.E. Morales. 2012. Spatial patterns of annual and interannual surface chlorophyll-*a* variability in the Peru-Chile System. Prog. Oceanogr., 92-95: 8-17.

Dong, C., J. McWilliams & A. Shchepetkin. 2007. Islands wakes in deep water. J. Phys. Oceanogr., 37: 962-981.

Doty, M.S. & M. Ogury. 1956. The island mass effect. J. Cons. Int. Explor. Mer, 22: 33-37.

Falkowski, P.G., D. Ziemann, Z. Kolber & P.K. Bienfang. 1991. Role of eddy pumping in enhancing primary production in the Ocean. Nature, 352(6330): 55-58.

Fuenzalida, R., W. Schneider, J. Garcés-Vargas & L. Bravo. 2008. Satellite altimetry data reveal jet-like dynamics of the Humboldt Current. J. Geophys. Res., 113, C07043, doi:10.1029/2007JC004684.

Gerrard, T.H. 1978. The wake of a cylindrical bluff bodies at low Reynolds number. Philos. Trans. Roy. Soc. London, 288(A): 351-382.

González-Ferrán, O. 1987. Evolución geológica de las islas chilenas en el Océano Pacífico. En: J.C. Castilla (ed.). Islas oceánicas chilenas: conocimiento científico y necesidades de investigaciones. Ediciones Universidad Católica de Chile, Santiago, pp. 37-54.

Hajek, E. & G. Espinoza. 1987. Meteorología, climatología y bioclimatología de las islas oceánicas chilenas. En: J.C. Castilla (ed.). Islas oceánicas chilenas: conocimiento necesidades científico y de investigaciones. Ediciones Universidad Católica de Chile, Santiago, pp. 55-83.

Hardy, J., A. Hanneman, M. Behrenfeldt & R. Horner. 1996. Environmental biogeography of near-surface phytoplankton in the southeast Pacific Ocean. Deep-Sea Res. I, 43: 1647-1659.

Hasegawa, D., M.R. Lewis & A. Gangopadhyay. 2009. How islands cause phytoplankton to bloom in their wakes. Geophys. Res. Lett., 36, L20605, doi:10.1029/2009GL039743.

Heywood, K.J., E.D. Barton & J.H. Simpson. 1990. The effects of flow disturbance by an oceanic island. J. Mar. Res., 48: 55-73.

Heywood, K.J., D.P. Stevens & G.R. Bigg. 1996. Eddy formation behind the tropical island of Aldabra. Deep-Sea Res. I, 43: 555-578.

Hormazábal, S., G. Shaffer & O. Pizarro. 2002. Tropical Pacific control of intraseasonal oscillations off Chile by way of oceanic and atmospheric pathways, Geophys. Res. Lett., 29, 6, doi:10.1029/2001GL 013481.

Hormazábal, S., G. Shaffer & O. Leth. 2004. Coastal transition zone off Chile. J. Geophys. Res-Oce., 109, C1, doi:10.1029/2003JC001956.

Hormazábal, S., G. Shaffer, J. Letelier & O. Ulloa. 2001. Local and remote forcing of sea surface temperature in the coastal upwelling system off Chile. J. Geophys. Res., 106: 16657-16672.

Karl, D.M., R.R. Bidigare & R.M. Letelier. 2001. Long-term changes in plankton community structure and productivity in the North Pacific subtropical Gyre: the domain shift hypothesis. Deep-Sea Res. II, 48: 1449-1470.

Landaeta, M.F. & L.R. Castro. 2004. Zonas de concen-tración de ictioplancton en el archipiélago de Juan Fernández, Chile. Cienc. Tecnol. Mar, 27(2): 43-53.

Laws, E.A., G.R., Ditullio & D.G. Redalje. 1987. High phytoplankton growth and production-rates in the north Pacific subtropical gyre. Limnol. Oceanogr., 32: 905-918.

Leth, O. & G. Shaffer. 2001. A numerical study of the seasonal variability in the circulation off central Chile. J. Geophys. Res., 106(C10): 22229-22248.

Mann, M.E. & J. Park. 1999. Oscillatory spatiotemporal signal detection in climate studies: a multiple-taper spectral domain approach. Adv. Geophys., 41: 1-131.

Marañon, E., P.M. Holligan, M. Varela, B. Mouriño & A.J. Bale. 2000. Basin-scale variability of phytoplankton biomass, production and growth in the Atlantic Ocean. Deep Sea Res. I, 47: 825-857.

Marañon, E., M.J. Behrenfeld, N. Gonzalez, B. Mouriño & M.V. Zubkov. 2003. High variability of primary production in oligotrophic waters of the Atlantic Ocean: uncoupling from phytoplankton biomass and size structure. Mar. Ecol. Prog. Ser., 257: 1-11.

Marra, J. & K.R. Heinemann. 1987. Primary production in the north Pacific central gyre-some new measurements based on C-14. Deep-Sea Res. I, 34: 1821-1829.

McClain, C.R., S.R. Signorini & J.R. Christian.2004. Subtropical gyre variability observed by ocean-color satellites. Deep-Sea Res. II, 51: 281-301.

McGillicuddy, D.J., L.A. Anderson, N.R. Bates, T. Bibby, K.O. Buesseler, C.A. Carlson & C.S. Davis. 2007. Eddy/Wind interactions stimulate extraordinary mid-ocean plankton blooms. Science, 316(5827): 1026.

Moraga, J., P. Lagos & W. Argandoña. 2010. Dinámica de las aguas costeras de Isla de Pascua. Cienc. Tecnol. Mar, 33(2): 5-16.

Nauw, J.J., H.M. van Aken, J.R.E. Lutjeharms & W.P.M. de Ruijter. 2006. Intrathermocline eddies in the southern Indian Ocean. J. Geophys. Res., 111, C03006. doi:10.1029/2005JC002917.

Parín, N.V. 1991. Fish fauna of the Nazca and Salas y Gómez submarine ridges, the easternmost outpost of the indo-west Pacific zoogeographic region. Bull. Mar. Sci., 49(3): 671-683.

Pizarro, G., V. Montecino, R. Astoreca, G. Alarcón, G. Yuras & L. Guzmán. 2006. Variabilidad espacial de condiciones bio-ópticas de la columna de agua entre las costas de Chile insular y continental, primavera 1999 y 2000. Cienc. Tecnol. Mar, 29(1): 45-58.

Porovic, J., C. Parada, B. Ernst, S. Hormazábal & V. Combes. 2012. Modelación de la conectividad de las subpoblaciones de la langosta de Juan Fernández (*Jasus frontalis*), a través de un modelo biofísico. Lat. Am. J. Aquat. Res., 40(3): 613-632.

Ras, J., H. Claustre & J. Uitz. 2008. Spatial variability of phytoplankton pigment distributions in the subtropical south Pacific Ocean: comparison between *in situ* and predicted data. Biogeosciences, 5: 353-369.

Sangrà, P., M. Auladell, A. Marrero-Díaz, J.L. Pelegrí, E. Fraile-Nuez, A. Rodríguez-Santana, J.M. Martín, E. Mason & A. Hernández-Guerra. 2007. On the nature of oceanic eddies shed by the Island of Gran Canaria. Deep-Sea Res. I, 54: 687-709.

Sepúlveda, J.I. 1987. Peces de las islas oceánicas chilenas. En: J.C. Castilla (ed.). Islas oceánicas chilenas: conocimiento científico y necesidades de investigaciones. Ediciones Universidad Católica de Chile, Santiago, pp. 227-245.

Signorini, S.R., C.R. McClain & Y. Dandonneau. 1999. Mixing and phytoplankton bloom in the wake of the Marquesas Islands. Geophys. Res. Lett., 26: 3121-3124.

Silva, N. 1992. Condiciones oceanográficas alrededor de Isla de Pascua, durante la primavera de 1979. Cienc. Tecnol. Mar, 15: 21-30.

Werdell, J. 2009. Global bio-optical algorithms for ocean color satellite applications: inherent optical properties algorithm workshop at ocean optics. Barga, Italy, 3-4 October 2008, EosTrans., 90(1): 4, doi:10.1029/ 2009EO010005.

Winn, C.D., L. Campbell, J.R. Christian, R.M. Letelier, D.V.Hedel, J.E. Dore, L. Fujieki & D.M. Karl. 1995. Seasonal variability in the phytoplankton community of the north Pacific subtropical gyre. Glob. Biogeochem. Cy., 9: 605-620.

Yuras, G., O. Ulloa & S. Hormazábal. 2005. On the annual cycle of coastal and open ocean satellite chlorophyll off Chile (18-40ºS). Geophys. Res. Lett., 32, L23604, doi:10.1029/2005GL023946.